WAVINESS OF THE SOUTHERN HEMISPHERE WINTERTIME POLAR AND SUBTROPICAL JETS

by

Jonathan E. Martin[1] and Taylor Norton[2]

[1]Department of Atmospheric and Oceanical Sciences
[2]Antarctic Meteorological Research Center
University of Wisconsin-Madison
Madison, WI 53706

Corr. Author: Jonathan E. Martin, jemarti1@wisc.edu

30   ABSTRACT
31
32
33   The recently developed average latitudinal displacement (ALD) methodology is applied

34 to assess the waviness of the austral winter subtropical and polar jets using three different

35 reanalysis data sets. As in the wintertime Northern Hemisphere, both jets in the Southern

36 Hemisphere have become systematically wavier over the time series and the waviness of each jet

37 evolves quite independently of the other during most cold seasons. Also, like its Northern

38 Hemisphere equivalent, the Southern Hemisphere polar jet exhibits no trend in speed (though it

39 is notably slower) while its poleward shift is statistically significant. In contrast to its Northern

40 Hemisphere counterpart, the austral subtropical jet has undergone both a systematic increase in

41 speed as well as a statistically significant poleward migration. Composite differences between

42 the waviest and least wavy seasons for each species suggest that the Southern Hemisphere's

43 lower stratospheric polar vortex is negatively impacted by unusually wavy tropopause-level jets

44 of either species. These results are considered in the context of trends in the Southern Annular

45 Mode as well as the findings of other related studies.

46

47 **KEYWORDS**: Southern Hemisphere, winter, polar jet, subtropical jet, waviness

48

1. Introduction

Consideration of changes in the behavior of the tropopause-level jet streams in a warming world has been catalyzed by the construction of long-period reanalysis data sets over the past three decades (Kalnay et al, 1996; Kistler et al., 2001; Kobayashi et al. 2015; Copernicus Climate Change Services [CS3], 2017). Recent analyses employing these data sets (e.g. Archer and Caldiera, 2008; Barnes and Screen, 2015; Gallego et al. 2005; Manney and Hegglin, 2018; Peña-Ortiz et al. 2013; Vavrus et al. 2017), in tandem with a number of studies based upon climate model output (e.g. Barnes and Polvani, 2013; Lorenz and DeWeaver, 2007; Miller et al. 2006; Yin, 2005), have produced a consensus view that poleward displacement of both jets accompanies warming. Along with an interest in latitudinal position, nearly all of the aforementioned studies have also addressed either observed and/or forecasted changes in the speed of the jet streams.

In a recent paper Martin (2021) offered a feature-based analysis of the *waviness* of the tropopause-level polar and subtropical jets during Northern Hemisphere winter (DJF). The analysis proceeded from the results of Christenson et al. (2017) that identified the isentropic layers that house the two species of jets during NH winter. He found that 1) the polar jet (POLJ) has undergone a statistically significant poleward migration over the time series, not matched by the subtropical jet (STJ), and 2) neither jet species exhibited a trend in its speed. Additionally, the analysis showed that both jets have become systematically wavier over the last 6 decades.

By virtue of its land/sea distribution, enhanced lower tropospheric warming at high latitudes of the NH, known as Arctic amplification, has recently emerged as a prominent signal of climate change (e.g., Serreze et al. 2009; Screen and Simmonds, 2013: and references therein). Francis and Vavrus (2012) were among the first to propose that changes in the undulatory nature

73 of the jet stream might be linked to Arctic amplification. This suggestion initiated a decade-long

74 debate on this issue (e.g. Barnes, 2013; Blackport and Screen, 2020; DiCapua and Coumou,

75 2016; Francis, 2017; Francis and Vavrus, 2015; Francis et al. 2018; Martineau et al. 2017, Screen

76 and Simmonds, 2013; Vavrus, 2018). As noted by Martin (2021), at least some of the

77 controversy and attendant lack of consensus surrounding this question (Barnes and Polvani,

78 2015) was nourished by the absence of a robust method of assessing the waviness of the

79 tropopause-level jets. The average latitudinal displacement (ALD) methodology introduced in

80 Martin (2021) (briefly described later) offers one possible remedy to this deficiency.

81   The principle mode of variability in the SH extratropical circulation is the Southern

82 Annular Mode (SAM, Limpasuvan and Hartmann, 1999; Gong and Wang, 1999; Thompson and

83 Wallace, 2000), a nearly zonally symmetric structure with coincident geopotential height

84 anomalies of opposite signs in Antarctica and the middle latitudes. In the decades prior to 2000,

85 the SH jets have shifted poleward and the SAM has tended toward positive polarity (e.g. Fogt

86 and Marshall, 2020). These coincident trends have been presumed to be a result of ozone

87 depletion. As the ozone recovers in the SH, simulations suggest a reversal of this trend may be

88 forthcoming (WMO, 2022). Spenberger et al. (2020) have questioned whether the associated jet

89 displacement also explains shifts in the storm tracks across the hemisphere. Instead they suggest

90 that SAM can be interpreted as a measure of the degree of coupling (or decoupling) between

91 Antarctica and the southern mid-latitudes.

92   Recently, considerable attention has been devoted to interrogating the zonally

93 asymmetric component of SAM (e.g. Fan 2007; Silvestri and Vera, 2009; Fogt et al. 2012; Rosso

94 et al. 2018; Campetelli et al. 2022). This asymmetric component is characterized by a wave-3

95 pattern (Goyal et al., 2021; Goyal et al., 2022; Campetelli et al. 2022) with maximum amplitude

96   at 250 hPa in the Pacific and may be determinative of the overall positive trend in the SAM over

97   the reanalysis era. Such a wave-3, tropopause-level signal is immediately suggestive of the

98   influence of the jets. These observations motivate consideration of direct measurement of the

99   waviness of the SH wintertime jets.

100   Despite a number of recent studies that consider aspects of the interannual variability of

101   the austral winter subtropical jet (e.g. Gillett et al., 2021; Maher et al. 2019), to our knowledge, a

102   study by Gallego et al. (2005) is the only one to consider direct measurement of the waviness of

103   the austral winter jets. They employed an objective method focused on identifying the

104   geostrophic streamline of maximum average velocity at 200 hPa (i.e. the jet core at that level) to

105   separately consider the behaviors of the STJ and POLJ. This method allowed consideration of

106   the jets as continuous features around the hemisphere and thus enabled a number of novel

107   analyses of their behavior and trends. With particular relevance to the present study, they

108   considered a zonal index computed as the difference between the maximum and minimum

109   latitude of the jet core (i.e. the streamline at the core of the jet) on each day. A similar metric,

110   termed DayMaxMin, was employed by Barnes (2013) in her consideration of the behavior of the

111   NH 500 hPa flow. Though insightful, such a metric does not comprehensively account for the

112   waviness created by the full collection of troughs and ridges around the hemisphere that

113   routinely characterizes the jets.

114   In this paper we apply the methodology of Martin (2021) to assess recent trends in the

115   waviness of the SH wintertime polar and subtropical jets. The method of identifying the austral

116   winter polar and subtropical jet locations in isentropic space is described in Section 2 along with

117   a description of the data sets used. Also included there is a short description of the method of

118   assessing waviness introduced in Martin (2021). In Section 3, elements of the long-term trend

119   and interannual variability of the waviness of the austral winter polar and subtropical jets are

120   presented along with differences between composites of the waviest and least wavy seasons for

121   each species. A summary and conclusions are offered in Section 4.

122

123   **2. Data and Methodology**

124

125   In the foregoing analysis, the zonal (u) and meridional (v) winds as well as temperature (T),

126   at 6 h intervals from three different reanalysis data sets are employed. 72 austral winters (JJA)

127   (1948-2019) of the National Centers for Environmental Prediction/National Center for

128   Atmospheric Research (NCEP/NCAR) reanalysis, at 17 isobaric levels to 10 hPa on a 2.5°

129   latitude-longitude grid (Kalnay et al., 1996; Kistlet et al., 2001) are used. We employ 62 winters

130   (1958-2019) of the Japanese 55-year (JRA-55) reanalysis with data on 60 vertical levels up to 0.1

131   hPa on a horizontal grid mesh of ~55 km (Kobayashi et al., 2015). Finally, the ERA5 reanalysis

132   data set on 137 vertical levels from the surface to 80 km with a grid spacing of 31 km covering

133   the period from 1979 to 2019 (Copernicus Climate Change Service [CS3], 2017) are used as

134   well. The waviness of the jets is assessed in the context of understanding their relationships to

135   the horizontal gradient of potential vorticity (PV) in prescribed isentropic layers. A similar

136   approach was taken with respect to the STJ in recent work by Maher et al. (2019). The first step

137   in the present analysis involves identification of the isentropic layers that house the austral winter

138   jets. This was accomplished empirically by identifying the isentropic level at which the

139   maximum wind speed was observed in each grid column (between 10 and 80°S) at each analysis

140   time in JJA over the 62-year time series of the JRA-55 data set. The use of isentropic space here

141   differs from the insightful approach taken by Manney et al. (2017) and Manney and Hegglin

142 (2018) which employed separate latitude and elevation criteria to differentiate between the STJ

143 and the POLJ. Of the three data sets employed in the present work, the JRA-55 was chosen for

144 this preliminary analysis step because both its length of time series as well as its horizontal and

145 vertical resolutions are between those characterizing the other two data sets employed here.

146 Following Koch et al. (2006) we only considered columns in which the integral average wind

147 speed exceeded 30 ms^{-1} in the 100-400 hPa layer. The resulting distribution is clearly tri-modal

148 with frequency maxima, and therefore separate jet features, approximately located in the 305-

149 320, 340-355, and 395-410K isentropic layers (Fig. 1a). The latter isentropic layer appears in the

150 lower stratosphere and is associated with the austral polar night jet (PNJ), which, being located

151 *above* the tropopause, is not a focus of the present analysis. Further separation of the STJ and

152 POLJ is achieved through reference to Fig. 2 of Gallego et al. (2005) which strongly implies that

153 the STJ sharply peaks near 30°S while the POLJ more broadly peaks around 50°S. Accordingly,

154 we further constrained the analysis to latitude bins 0-40°S for the STJ and 40 to 65°S for the

155 POLJ. With this additional refinement, the analysis identifies the STJ in the 340-355K isentropic

156 layer and the POLJ in the 310-325K isentropic layer (Fig. 1b). Similar analyses of the other two

157 data sets (not shown) revealed the robustness of this result. It is important to note that 53.8% of

158 all qualifying columns (to 380K) in the 0-40°S bin (STJ) were in the 340-355K layer while

159 46.8% of all qualifying columns in the 40-65°S bin (POLJ) were in the 310-325K layer

160 supporting the isentropic assignments for the two species mentioned previously. It is

161 immediately apparent, consistent with prior analyses (e.g. Bals-Elsholz et al. 2001, Nakamura

162 and Shimpo 2004, Gallego et al. 2005), that the STJ is the dominant jet feature in the southern

163 winter.

164   The analysis method to be used here involves assessment of the circulation which

165   requires calculation of contour length. As a result, fair comparison among the different data sets

166   requires adoption of a uniform grid spacing. Consequently, all three data sets were bilinearly

167   interpolated onto isentropic surfaces at 5K intervals (from 280 to 380K) and 2.5° latitude-

168   longitude grid spacing using programs within the General Meteorological Analysis Package

169   (GEMPAK) (desJardins et al., 1991). The average PV and average zonal and meridional wind

170   speeds in both the polar jet (310:325K) and subtropical jet (340:355K) layers were then

171   calculated from the four times daily data for each day in each of the three time series.

172   As reviewed in Martin (2021), consideration of the quasi-geostrophic potential vorticity

173   (QGPV), following Cunningham and Keyser (2004), demonstrates that local maxima in the

174   cross-flow gradient of QGPV are collocated with maxima in the geostrophic wind speed. In the

175   Southern Hemisphere, the jets lie on the high PV edge of this PV gradient. By searching through

176   daily average isertels from -0.5 to -5.0 at 0.1 PVU intervals (1 PVU = 10^{-6} m^2 K kg^{-1} s^{-1}), the

177   analysis identifies a "core isertel" along which the circulation per unit length (i.e. average speed)

178   is maximized in the separate POLJ (310:325K) and STJ (340:355K) isentropic layers for every

179   day in each of the time series. This core isertel is, by design, an analytical proxy for the jet core.

180   A glimpse into the fidelity of this method in identifying the meandering cores of the POLJ and

181   STJ jets is illustrated in Fig. 2. In each case the objectively identified core isertel, in black, lies

182   very near, or at, the center of the analyzed isotach maxima around the hemisphere with

183   physically defensible exceptions. For instance, the red dashed lines in Fig. 2b indicate portions

184   of the bold black line in Fig. 2d (i.e. the overlying STJ core) suggesting that those portions of the

185   isotach maxima in Fig. 2b that are somewhat removed from the POLJ core isertel are the lower

186   portions of the overlying STJ core. Similarly, an extensive isotach maxima region in Fig. 2d has

187   a blue dashed line, a portion of the bold black line in Fig. 2b, slicing through it. This region,

188   well poleward of the STJ core isertel, is clearly the upper portion of the underlying POLJ core.

189   Figure 3a shows the average latitude for the core isertels of each jet species from each of the

190   three reanalyses data sets used in the study. The analyses return essentially identical results for

191   the core isertel of the STJ and very nearly identical results for the POLJ. Superimposing the

192   NCEP-NCAR reanalysis' JJA average 200 hPa isotachs on top of the STJ core isertels (Fig. 3b)

193   illustrates the fact that the average core isertel accurately represents the axis of the average STJ.

194   The relationship is also strong between the POLJ core isertels and the 700 hPa average isotachs

195   (Fig. 3c).

196   The waviness of each jet is assessed by calculating a hemispheric average of the meridional

197   displacements of the core isertel from its equivalent latitude – the northern extent of a polar cap

198   whose area is equal to the area enclosed by the core isertel. This metric is referred to as the

199   average latitudinal displacement (ALD). The method does not require that the core isertel be the

200   same in both jet layers on a given day, nor that it be the same from day-to-day in a given jet

201   layer. Consequently, it is important to examine its distribution in each jet layer over the entire

202   time series. Figure 4 portrays the frequency of occurrence of the core isertels in both the STJ

203   and POLJ layers for each of the three time series. The STJ core isertels peak between -1.95 and -

204   2.1 PVU across the three data sets. Considering all three data sets, 81.5% of all JJA days exhibit

205   a core isertel between -1 and -3 PVU in the STJ layer. The POLJ distribution is shifted toward

206   higher PV values. Overall, 74.8% of JJA days had a core isertel between -1 and -3 PVU in the

207   POLJ layer. The frequency of occurrence in the several isertelic bins for each species of SH jet

208   match quite well with what Martin (2021) found for the NH wintertime jets, even when

209   accommodating for the different isentropic layer for the austral POLJ.

210

3. Analysis

212

The JJA seasonal average latitudinal displacement (ALD) of each jet is calculated as a

92-day average of the daily ALD in each cold season. The results are shown in Fig. 5. It is

instantly clear that, as in the NH, the POLJ is wavier than the STJ and that both jets have become

systematically wavier over the 62-year JRA-55 time series with $p < 0.004$ for both time series (a

one-sided Student's t-test was employed). Interestingly, the austral winter STJ is less wavy than

its NH counterpart but the waviness of both has increased identically at 0.005 deg/yr (0.0125

deg/yr for NCEP since 1958 and -0.001 deg/yr for ERA-5). The winter POLJ in the SH is, on

the other hand, wavier than in the NH and is trending faster (0.017 versus 0.009 deg/yr; 0.023

deg/yr for NCEP since 1958 and 0.009 deg/yr for ERA-5) than its NH complement. Daily time

series of the ALD of each jet can also be examined to determine the extent to which the waviness

of the two jets covaries. Figure 6 illustrates the POLJ and STJ daily ALDs for 1999 from each of

the three data sets. The low correlation between the waviness of the two species in this example

year represents the rule rather than the exception. All told, more than 93% of the STJ and POLJ

ALD seasonal time series constructed for this study are correlated with magnitudes less than 0.3.

This result strongly suggests that the waviness of the two species evolves independently.

By definition, the average wind speed along the chosen core isertel on any given day

represents the average jet speed for that species on that day. Time series of seasonal average jet

core wind speeds for the wintertime STJ and POLJ in both hemispheres are shown in Fig. 7. As

in the NH winter (Martin, 2021), the austral POLJ shows almost no trend in jet core speed and

the slight change is not statistically significant. Notably, however, the SH POLJ is ~6 m s^{-1}

233   slower on average than its NH equivalent. Aside from the fact that the NCEP reanalysis is quite

234   different from the JRA-55 until about 1970, the austral winter STJ exhibits a robust, and

235   statistically significant (p-value < 0.001), increase in speed over the JRA-55 time series – in clear

236   contrast to its NH counterpart. It is also apparent that the SH STJ is slightly weaker but less

237   interannually variable than the NH STJ.

238   Another characteristic of interest that emerges directly from the ALD analysis method is

239   the daily value of the jet core's equivalent latitude which closely approximates its zonally

240   averaged position. Consequently, it is straightforward to construct a time series of the seasonal

241   average equivalent latitudes of the two species of jets, shown in Fig. 8. Again, as in the NH, the

242   poleward shift of the SH POLJ is occurring three times faster than that exhibited by the STJ. In

243   contrast to the situation in the NH, however, the slight poleward displacement of the SH STJ *is*,

244   like that of the POLJ, statistically significant (*p*-values for the POLJ and STJ are <0.001 and

245   0.002, respectively). It is interesting to note that while the SH STJ is located at a roughly similar

246   latitude as the NH STJ throughout the time series, the SH POLJ is ~4° further poleward during

247   winter than the NH POLJ. Overall, a much more systematic and dramatic poleward migration of

248   the two jets has occurred over the last 6 decades in SH winter as compared to NH winter.

249   Next we consider aspects of the analysis in the context of the SAM. Figure 9 shows a

250   histogram of the JJA average SAM index (calculated after Gong and Wang (1999))

251   superimposed upon the average JJA ALD from the JRA-55 reanalysis. The tendency toward

252   positive SAM over the time series appears to be reflected in the increase in ALD. However, the

253   correlation between the two time series is 0.053 suggesting almost no relationship exists between

254   the two.

255   In order to investigate the relationship of ALD to extremes in the polarity of the SAM

256   index, the three winter months with the most positive and most negative SAM extremes since

257   1979 were considered. The core isertels of the POLJ (from the JRA-55 reanalysis) for each of

258   these three months is portrayed in Fig. 10. Positive extremes of SAM (Figs. 10a, c, and e) show

259   a clear poleward encroachment of the SH polar jet while negative extremes (Figs. 10b, d, and f)

260   suggest the opposite. There appears to be no systematic connection, however, between extremes

261   in SAM and the waviness of the POLJ as quantified by ALD.

262   Thus far the analysis has presented elements of the seasonal average behavior of the

263   austral winter jet species. The methodology, of course, allows for evaluation of daily time series

264   of ALD as well and, in fact, such an analysis underlies the presentation in Fig. 6. Using such

265   daily time series, identification of the waviest and least wavy seasons for each jet species since

266   1979 is accomplished by summing the daily departures from calendar-day average ALD over the

267   92 days of each cold season. The list of such seasonally integrated departures from average

268   waviness for each species of jet for each reanalysis data set is shown in Table 1. From this list,

269   the 5 waviest and 5 least wavy seasons for each jet species were selected to construct composites

270   of geopotential height at several isobaric levels employing the JRA-55 data. In the foregoing

271   analysis, height differences are obtained by subtracting values associated with the composite

272   least wavy seasons from those associated with the composite waviest seasons.

273   Figure 11a shows the 500 hPa geopotential height differences between the waviest and

274   least wavy POLJ seasons. Wavy POLJ years are characterized by positive height anomalies over

275   the continent and adjacent to its east and west coasts with belts of negative anomalies in a

276   crescent stretching from southwest of Chile and then extending from the east coast of South

277   America to southern Africa toward Australia, suggestive of a negative SAM. The strongest

278   negative height anomalies in such seasons occur west of South Africa implying a slight

279   weakening of the zonal winds just south of the Cape of Good Hope. Meanwhile wavy STJ years

280   exhibit negative composite height differences in roughly the same locations as the positive

281   composite differences just described for wavy POLJ years (Fig. 11b), suggestive of a positive

282   SAM. These composite difference patterns strengthen slightly at 250 hPa (Fig. 12) suggesting an

283   equivalent barotropic structure to the tropospheric portion of the difference fields.

284   The difference fields at 50 hPa imply that the waviness of both jets exerts an

285   influence on the strength of the austral polar vortex in the lower stratosphere. The anomalous

286   height field associated with wavy POLJ years (Fig. 13a) suggests a broad, though modest,

287   anticyclonic circulation anomaly just off the pole in the Western Hemisphere. Such a

288   perturbation flow would appear to interfere with the establishment and/or persistence of strong

289   vortex flow in the same location. Wavy STJ seasons also impose a dipole of positive heights the

290   axis of which stretches from Cape Horn to East Antarctica (Fig 13b). Such a configuration

291   implies that the polar vortex is both weaker and displaced off the pole in winters with wavy

292   STJs. Thus, the analysis suggests that in winters characterized by unusually wavy jets of either

293   species, the SH polar vortex is likely weaker than normal. Further investigation of this intriguing

294   implication is the subject of ongoing work.

295

296   **4. Summary**

297

298   The analysis presented here extends the application of a method developed by Martin

299   (2021) to assess the waviness of the tropopause-level jets to analysis of the austral winter polar

300   and subtropical jets. The analysis demonstrates that both jets have become systematically wavier

301   over the past 60+ years. In addition, as in the NH, the waviness of the two species of austral

302   winter jets is largely uncorrelated suggesting little systematic influence of one on the other

303   throughout the season. Along with these similarities, there appear to be some fundamental

304   asymmetries in the behavior of the wintertime tropopause-level jets between the hemispheres.

305   The austral POLJ, like its NH counterpart, has exhibited no trend in its average speed over the

306   time series, though it is notably slower than its NH wintertime equivalent. The STJ, on the other

307   hand, has roughly the same speed as that in the NH winter but, unlike its NH counterpart, has

308   undergone a systematic, statistically significant increase in its core speed since ~1960.

309   Additionally, as opposed to the situation in the NH where only the POLJ migration toward to

310   pole is statistically significant, **both** SH jets exhibit a significant poleward creep with the POLJ

311   encroachment occurring at ~3x the rate of that characterizing the STJ.

312   The observed poleward migration of the STJ reported here is consistent with the analysis

313   of CMIP5 simulations of historical and projected changes to the SH wintertime STJ by Chenoli

314   et al. (2017). Though the present work employs a similarly dynamical definition of the STJ as

315   that used in the study by Maher et al. (2019), they found no evidence of a poleward shift of the

316   SH wintertime STJ. We suggest that the emphasis on empirically identifying a core isertel,

317   rather than the maximum gradient of θ on a predetermined isertelic surface (i.e. 2 PVU as the

318   dynamic tropopause) may account for this difference.

319   Finally, circulation differences between the waviest and least wavy POLJ and STJ

320   seasons are manifest in both the troposphere and lower stratosphere. In the troposphere the

321   signals are not as coherent in the SH as they were revealed to be in the NH (Martin 2021).

322   Interestingly, the analysis implies that when either the POLJ or STJ is wavier than normal in a

323   given winter, the lower stratospheric polar vortex is negatively impacted. Again, this is different

324   from the behavior of the NH polar vortex in the face of extremes in waviness.

325   The results presented here, combined with those in Martin (2021), demonstrate that in

326   both hemispheres a wavier than normal STJ during winter serves to weaken the lower

327   stratospheric polar vortex. Though, as suggested by the analysis supporting Fig. 6, the STJ and

328   POLJ do not appear to influence one another systematically, there are still instances in which the

329   waviness of the two jets can be phased so as to promote intense interactions. Daily perusal of

330   hemispheric synoptic maps suggests that such instances of jet interaction often lead to intense

331   lower tropospheric cyclogenesis events. Current research is examining whether such jet

332   interaction-induced cyclogenesis events from specific seasons systematically correspond to

333   episodes of polar vortex weakening.

334

335   COMPETING INTERESTS: The contact author has declared that none of the authors has any

336   competing interests.

337

338   AUTHOR CONTRIBUTIONS: J. Martin completed the ALD analysis and did all the writing,

339   figure drafting and preparation of the manuscript for submission. T. Norton performed the

340   analysis that determined the POLJ and STJ isentropic housings during SH winter.

341

342   ACKNOWLEDGEMENTS: This work was supported by the National Science Foundation under

343   grants ATM-1640055 and NSF-2055667. JRA-55 data available from the Research Data

344   Archive at the National Center for Atmospheric Research. The authors would like to thank Prof.

345   Andrea A. Lopez-Lang for helpful comments and suggestions.

REFERENCES

Archer, C. L., and K. Caldeira, 2008: Historical trends in the jet stream. *Geo. Res. Let.*, **35**(8).

Bals-Elsholz, T. M., E. H. Atallah, L. F. Bosart, T. A. Wasula, M. J. Cempa, and A. R. Lupo, 2001: The wintertime Southern Hemisphere split jet: Structure, variability, and evolution. *J. Climate*, 14, 4191-4215.

Barnes, E. A., 2013: Revisiting the evidence linking Arctic amplification to extreme weather in midlatitudes. *Geophys. Res. Let.*, **40**, 4734-4739.

_____, and L. Polvani, 2013: Response of the midlatitude jets, and of their variability, to increased greenhouse gases in the CMIP5 models. *J. Climate*, 26, 7117-7135.

_____, and J. A. Screen, 2015: The impact of Arctic warming on the midlatitude jet-stream: Can it? Has it? Will it? *WIREs Clim Change*, **6**, 277–286. doi: 10.1002/wcc.337.

Blackport, R., and J. A. Screen, 2020: Insignificant effect of Arctic amplification on the amplitude of midlatitude atmospheric waves. *Science advances*, *6*(8), p.eaay2880.

Campitelli, E., L. B. Diaz, and C. Vera, 2021: Assessment of zonally symmetric and asymmetric components of the Southern Annular Mode using a novel approach. *Clim. Dyn.*, **58**, 161-178.

369 Chenoli, S. N., M. Y. Ahmad Mazuki, J. Turner, & A. A. Samah, 2017: Historical and projected

370   changes in the Southern Hemisphere sub-tropical Jet during winter from the CMIP5

371   models. *Clim. Dyn.*, **48,** 661-681.

372

373 Christenson, C. E., J. E. Martin, and Z. J. Handlos, 2017: A synoptic-climatology of Northern

374   Hemisphere, cold season polar and subtropical jet superposition events. *J. Climate*, **30**,

375   7231-7246.

376

377 Copernicus Climate Change Service (C3S) (2017): ERA5: Fifth generation of ECMWF

378   atmospheric reanalyses of the global climate. Copernicus Climate Change Service

379   Climate Data Store (CDS), *March 2020,* https://cds.climate.copernicus.eu/cdsapp#!/home

380

381 Cunningham, P., and D. Keyser, 2004: Dynamics of jet streaks in a stratified quasi-geostrophic

382   atmosphere: Steady-state representations. *Quart. J. Roy. Meteor. Soc.,* **130,** 1579-1609.

383

384 desJardins, M. L., K. F. Brill, and S. S. Schotz, 1991: GEMPAK 5 Part I—GEMPAK 5

385   programmer's guide. National Aeronautics and Space Administration. [Available from

386   Scientific and Technical Information Division, Goddard Space Flight Center,

387   Greenbelt, MD 20771.].

388
389 DiCapua G., and D. Coumou,2016: Changes in the meandering of the Northern Hemisphere

390   circulation. *Environ. Res. Lett*., **11**, 094028, doi:10.1088/1748-9326/11/9/094028.

391

392 Fan, K.: Zonal asymmetry of the Antarctic Oscillation. *Geophys. Res. Lett*.,

393 https://doi.org/10.1029/2006GL028045.

394

395 Fogt, R. L., J. M. Jones, and J. Renwick, 2012: Seasonal zonal asymmetries in the Southern

396  Annular Mode and their impact on regional temperature anomalies. *J. Climate*, **25**, 6253-

397  6270.

398

399 Fogt, R. L. and G. J. Marshall, 2020: The Southern Annular Mode: Variability, trends, and

400  climate impacts across the Southern Hemisphere. *WIREs Climate Change*, **11(4)**:e652.

401  https://doi.org/10.1002/wcc.652.

402

403 Francis, J. A., 2017: Why are Arctic linkages to extreme weather still up in the air?. *Bull. Amer.*

404  *Meteor. Soc.,* **98**, 2551-2557.

405
406 _____, and S. J. Vavrus, 2012: Evidence linking Arctic amplification to extreme weather in mid-

407  latitudes. *Geophys. Res. Let*., **39**, L06801, doi:10.1029/2012GL051000.

408

409 _____, and _____, 2015: Evidence for a wavier jet stream in response to rapid Arctic warming.

410  *Environ. Res. Lett*. **10**, 014005, doi:10.1088/1748-9326/10/1/014005.

411

412 ______, N, Skific, and S. J. Vavrus, 2018: North American weather regimes are becoming more

413  persistent: Is Arctic amplification a factor? *Geophys Res.Lett*.,

414  https://doi.org/10.1029/2018GL080252.

415

416 Gallego, D., P. Ribera, R. Garcia-Herrera, E. Hernandez, and L. Gimeno, 2005: A new look for

417   the Southern Hemisphere jet stream. *Climate Dyn*., **24**, 607-621.

418

419   Gillett, Z. E., H. H. Hendon, J. M. Arblaster, and E.-P. Lim, 2021: Tropical and extratropical

420   influences on the variability of the Southern Hemisphere wintertime subtropical jet. *J.*

421   *Climate*, **34**, 4009-4022.

422

423   Gong, D., and S. Wang, 1999: Definition of Antarctic oscillation index. *Geophys. Res. Lett*., **26**,

424   459-462.

425

426   Goyal, R., M. Jucker, A. Sen Gupta, H. H. Hendon, and M. H. England, 2021: Zonal wave 3

427   pattern in the Southern Hemisphere generated by tropical convection. *Nat. Geosci*., **14**,

428   732-738.

429

430   ____, _____, _____, and M. H. England, 2022: A new zonal wave-3 index for the Southern

431   Hemisphere. *J. Climate*, **35**, 5137-5149.

432

433   Kalnay, E. and co-authors, 1996: The NCEP/NCAR 40-year reanalysis project. *Bull. Amer.*

434   *Meteor. Soc*.,   **77**, 437-470.

435

436   Kistler, R. and co-authors, 2001: The NCEP-NCAR 50-Year reanalysis: Monthly means CD-

437   ROM and documentation. *Bull. Amer. Meteor. Soc*., **82**, 247-267.

438

439   Kobayashi, S., Y. Ota, Y. Harada, A. Ebita, M. Moriya, H. Onoda, K. Onogi, H. Kamahori, C.

440   Kobayashi, H. Endo, K. Miyaoka, and K. Takahashi, 2015: The JRA-55 reanalysis:

441   General specifications and basic characteristics. *J. Meteor. Soc. Japan*, **93**, 5-48.

442

443   Koch, P., H. Wernli, and H. C. Davies, 2006: An event-based jet-stream climatology and

444   typology. *Int. J. Climatology*, **26**, 283-301.

445

446   Limpasuvan, V., and D. L. Hartmann, 1999: Eddies and the annular modes of climate

447   variability. *Geophys. Res. Lett.*, **26**, 3133–3136.

448

449   Lorenz, D. J., and E. T. DeWeaver, 2007: Tropopause height and zonal wind response to global

450   warming in the IPCC scenario integrations. *J. Geophys. Res: Atmos.*, **112**(D10).

451

452   Maher, P., M. E. Kelleher, P. G. Sansom, and J. Methven, 2020: Is the subtropical jet shifting

453   poleward?. *Clim. Dyn.*, **54**, 1741-1759.

454

455   Manney, G.L., M. I. Hegglin, Z. D. Lawrence, K. Wargan, L. F. Millán, M. J. Schwartz, M. L.

456   Santee, A. Lambert, S. Pawson, B. W. Knosp, and R. A. Fuller, 2017: Reanalysis

457   comparisons of upper tropospheric–lower stratospheric jets and multiple

458   tropopauses. *Atmos. Chem. and Phys.*, **17**, 11541-11566.

459

460   Manney, G. L., and M. I. Hegglin, 2018: Seasonal and regional variations of long-term changes

461   in upper-tropospheric jets from reanalyses. *J. Climate*, **31**, 423-448.

462

463   Martin, J. E., 2021: Recent trends in the waviness of the Northern Hemisphere wintertime polar

464   and subtropical jets. *JGR Atmos.*, https://doi.org/10.1029/2020JD033668.

465

466   Martineaux, P., G. Chen, and D. A. Burrows, 2017: Wave events: Climatology, trends, and

467   relationship to Northern Hemisphere blocking and weather extremes. *J. Climate*, **30**,

468   5675-5697.

469

470   Matsuno, T., 1971: A dynamical model of the stratospheric sudden warming. *J. Atmos. Sci., 28*,

471   1479-1494.

472

473   Miller, R. L., G. A. Schmidt, and D. T. Shindell, 2006: Forced annular variations in the 20th

474   century Intergovernmental Panel on Climate Change Fourth Assessment Report models.

475   *J. Geophys. Res.*, **111**, D18101, doi:10.1029/2005JD006323.

476

477   Nakamura, H., and A. Shimpo, 2004: Seasonal variations in the Southern Hemisphere storm

478   tracks and jet streams as revealed in a reanalysis data set. *J. Climate*, **17**, 1828-1844.

479

480   Peña-Ortiz, C., D. Gallego, P. Ribera, P. Ordonez, and M. D. C. Alvarez-Castro, 2013: Observed

481   trends in the global jet stream characteristics during the second half of the 20th century,

482   *J. Geophys. Res. Atmos.*, **118,** 2702–2713, doi:10.1002/jgrd.50305.

483

484   Rosso, F. V., N. T. Boiaski, S. E. T. Ferraz, and T. C. Robles, 2018: Influence of the Antarctic

485   oscillation on the South Atlantic convergence Zone. *Atmosphere*, *9*(11), 431.

486

487 Screen, J. A., and I Simmonds, 2013: Exploring links between Arctic amplification and mid-

488   latitude weather. *Geophys. Res. Lett.*, https://doi.10.1002/grl.50174.

489

490 Serreze, M.C., A. P. Barrett, J. C. Stroeve, D.N Kindig. and M.M. Holland, 2009: The

491   emergence of surface-based Arctic amplification. *Cryosphere*, **3**, 11-19.

492

493 Silvestri, G., and C. Vera, 2009: Nonstationary impacts of the Southern Annular Mode on

494   Southern Hemisphere climate. *J. Climate*, **22**, 6142–6148.

495

496 Spensberger, C., M. J. Reeder, T. Spengler, and M. Patterson, 2020: The connection between the

497   Southern Annular Mode and a feature-based perspective on Southern Hemisphere

498   midlatitude winter variability. *J. Climate*, **33**, 115,129.

499

500 Thompson, D., and J. Wallace, 2000: Annular modes in the extratropical circulation. Part I:

501   Month-to-month variability. *J. Climate.*, **13**, 1000-1016.

502

503 Vavrus, S. J., 2018: The influence of Arctic amplification on mid-latitude weather and climate.

504   *Curr. Clim. Change. Rep.*, **4**, 238-249.

505

506 _____, F. Wang, J. E. Martin, J. A. Francis, Y. Peings, and J. Cattiaux, 2017: Changes in North

507   American circulation and extreme weather: Influence of arctic amplification and

508   Northern Hemisphere snow cover. *J. Climate* , **30**, 4317-4333.

509

510 WMO. 2022. *Executive summary. Scientific assessment of ozone depletion: 2022, GAW report*

511   *no. 278*. Geneva, Switzerland: WMO

512 Yin, J. H., 2005: A consistent poleward shift of the storm tracks in simulations of 21st century

513   climate. *Geophys. Res. Let.*, **32**, L18701,doi:10.1029/2005GL023684.

514

	POLJ			STJ		
	NCEP	*JRA-55*	*ERA5*	*NCEP*	*JRA-55*	*ERA5*
1979	-45.416403	-19.684881	-64.232707	-3.7754167	11.1345645	0.70639878
1980	-59.380403	-58.393881	-63.657707	-3.2564167	4.47656452	-0.8576012
1981	18.8845972	36.4021194	21.8872927	-4.4154167	5.17956452	-2.2326012
1982	-24.813403	3.63785707	-15.198707	41.2785833	16.1355645	10.5773988
1983	-16.281403	35.8650731	-15.658707	-18.131417	-10.037435	-21.992601
1984	-14.954403	4.06711936	-6.9887073	15.8335833	19.8715645	11.5133988
1985	4.02659722	10.3371194	-20.535707	54.3615833	38.7185645	21.4393988
1986	24.2525972	43.6271194	20.5902927	-6.9904167	0.00256452	-10.285601
1987	62.9565972	77.0631194	16.8692927	-8.9194167	0.57256452	-9.2566012
1988	-2.5614028	-7.4278806	-35.518707	-1.9554167	2.34556452	-5.2936012
1989	-33.646403	9.93808658	-16.752707	35.2235833	29.6575645	19.4843988
1990	21.8045972	40.1761194	5.93129268	28.6225833	8.32356452	-0.0366012
1991	98.1615972	104.846187	79.9922927	15.9005833	13.6185645	10.0163988
1992	-31.301403	-26.480881	-43.682707	23.9145833	30.1255645	22.5733988
1993	45.9685972	64.4221194	23.6692927	-5.4784167	7.54756452	-0.9296012
1994	-29.454403	-32.656881	-69.886707	51.5895833	30.9815645	21.4813988
1995	-22.226403	-20.908881	-47.179707	-5.1054167	-12.989435	-16.721601
1996	80.0555972	96.1361194	86.8222927	-2.3444167	-10.092435	-11.395601
1997	68.8895972	57.6655297	78.5282927	2.23058333	-8.3644355	-11.693601
1998	-27.166403	-32.68934	-70.988707	18.5915833	-2.3754355	-7.9706012
1999	36.1115972	-22.593881	-44.562707	3.60158333	-23.970435	-32.015601
2000	57.1715972	17.3883325	16.0832927	49.9395833	18.8905645	12.2183988
2001	51.6315972	26.2991194	8.28429268	46.9905833	7.20656452	1.48939878
2002	30.0675972	35.9181194	21.4212927	65.2545833	47.0115645	40.0813988
2003	70.6935972	52.1291194	24.5692927	12.5915833	-3.7804355	-11.507601
2004	27.8395972	-18.835881	-31.660707	39.5535833	19.0855645	13.4163988
2005	48.0095972	26.0351194	-2.9987073	-10.510417	-21.297435	-26.212601
2006	76.9665972	27.7838267	24.9342927	29.3135833	-2.1904355	-10.139601
2007	60.9595972	55.4256292	46.9952927	38.6865833	17.2975645	14.1103988
2008	67.6425972	67.2851194	66.7882927	-4.0874167	-21.790435	-25.102601
2009	69.9215972	17.7955696	23.8622927	22.6285833	-4.6854355	-8.0676012
2010	41.5965972	13.4191194	3.93329268	31.9945833	16.0065645	11.1233988
2011	118.932597	111.764119	79.1722927	11.7745833	-5.6934355	-8.7496012
2012	38.3955972	9.84011936	-2.5287073	54.8005833	14.8235645	-1.2216012
2013	32.3355972	-0.7048806	-14.266707	67.4165833	25.3645645	13.6133988
2014	52.2325972	45.4011194	-60.736707	40.1415833	20.9895645	6.32532378
2015	65.0135972	38.0481194	18.8882927	14.6575833	1.69656452	-1.7356012
2016	51.9375972	19.3210046	15.3602927	22.3815833	2.71556452	-0.3676012
2017	15.4975972	-14.224881	-38.558707	30.2145833	2.97356452	-2.2008762
2018	70.8755972	21.0891194	3.86429268	3.15258333	-7.7994355	-11.277601
2019	68.5365972	5.97811936	-22.852707	58.1465833	21.7315645	7.09439878

TABLE 1 Integrated seasonal departures from average ALD (degrees) for polar and subtropical jets from the three reanalysis data sets employed in this work. Gray (light blue) shading representes one of the top 5 waviest (least wavy) seasons.

515

516   FIGURE CAPTIONS

517

518   Fig. 1 (a) Distribution of grid-column maximum wind speeds found in 5K isentropic layers from

519   10 - 80°S for every 6h analysis time in JJA from 1958-2019 from the JRA-55 reanalysis. (b) As

520   for Fig. 1a except limited to (i) grid-columns in which the integral average wind speed from 400

521   to 100 hPa exceeded 30 m s^{-1} and (ii) to latitudes 0 - 40°S for the STJ and (iii) latitudes 40 to

522   65°S for the POLJ.

523

524   Fig. 2 (a) Isotachs of the daily averaged wind speed (contoured every 10 m s^{-1} and shaded above

525   30 m s^{-1}) and the core isertel (bold black line) in the 310:325K isentropic layer on 13 July 1995

526   from the JRA-55 reanalysis data. The core isertel value is -1.3 PVU. (b) As in (a) but for 24

527   August 2001. Core isertel value is -2.0 PVU. Dashed red line indicates portion of the core

528   isertel from the overlying STJ layer (depicted in Fig. 2d). (c) As in (a) but for wind speeds and

529   core isertel in the 340:355K isentropic layer on 13 July 1995. Core isertel value is -3.6 PVU. (d)

530   As in (c) but for 24 August 2001. Core isertel value is -1.4 PVU. Dashed blue line indicates a

531   portion of the core isertel from the underlying POLJ layer (depicted in Fig. 2b). See text for

532   further explanation.

533

534   Fig. 3 (a) Solid (dashed) lines are the positions of the average core isertels of the STJ (POLJ)

535   from each of the three reanalyses employed in this study. The different reanalyses are color

536   coded. (b) Thick solid lines are the positions of the average core isertels for the STJ from each

537   of the reanalyses superimposed with JJA average 200 hPa isotachs from the NCEP-NCAR

538   reanalysis. (c) Thick dashed lines are the positions of the average core isertels for the POLJ

539   superimposed with JJA average 700 hPa isotachs from the NCEP-NCAR reanalysis.

540

541   Fig. 4 Frequency of occurrence of the core isertel value for each reanalysis time series in (a) the

542   STJ layer and (b) the POLJ layer. Solid blue, red and green lines in (a) and (b) are the SH

543   distributions from the NCEP, JRA55 and ERA5, respectively. The dashed blue, red and green

544   lines are the NH distributions from the NCEP, JRA55 and ERA5 reanalyses, respectively. In (b),

545   the NH distributions are from the 315:330K layer which houses the POLJ in the boreal winter.

546   Thin blue, red and green lines in (a) and (b) indicate the peak values of the core isertel in each

547   layer from each data set. Isertel values are given in potential vorticity units (PVU,

548   $1 \text{ PVU} = 10^6 \text{ K m}^2 \text{ kg}^{-1} \text{ s}^{-1}$), and are multiplied by -1 for the NH values.

549

550   Fig. 5 Seasonal average ALD (in degrees) of the SH wintertime subtropical and polar jets for

551   each cold season in the three reanalysis time series. The polar jet values are in the three shades

552   of blue while the subtropical jet values are in the three three shades of red. The dashed black line

553   through each time series represents the trend line for each (derived from the JRA-55 time series)

554   and is significant at the 96% level. Gray lines are the boreal winter ALD analysis from Fig. 6 of

555   Martin (2021).The "YEAR" on the abscissa indicates the year in which December of that cold

556   season occurred.

557

558   Fig. 6 Time series of the daily ALD of the polar (blue lines) and subtropical (red lines) jets from

559   the (a) NCEP-Reanalysis, (b) JRA-55, and (c) ERA5 data sets for austral winter 1999. The

560   correlation between the two times series from each data set is indicated.

561

562   Fig. 7 Seasonal average **U** along the core isertel for the subtropical (red lines) and polar (blue

563   lines) jets from each of the three SH reanalysis data sets. The thin black lines are trend lines for

564   each time series from the JRA-55 data. Gray lines are the equivalent boreal winter **U** analysis

565   from Fig. 9 of Martin (2021).

566

567   Fig. 8 Time series of the seasonal average equivalent latitude of the polar (blue lines) and

568   subtropical (red lines) jets from the three different SH reanalysis data sets. The thin black lines

569   are the trend lines (from the JRA-55 data) and are significant above the 99% leve for both jet

570   species. Gray lines are the boreal winter equivalent latitude analysis from Fig. 10 of Martin

571   (2021).

572

573   Fig. 9 JJA average SAM index (histogram) from NCEP's Climate Prediction Center. The index

574   is calculated by projecting the daily 700 hPa geopotential height anomalies poleward of 20S onto

575   the leading pattern of the Antarctic Oscillation (AAO) ofGong and Wang (1999). Black solid

576   line is theJJA average ALD of the POLJ from the JRA-55 reanalysis.

577

578   Fig. 10 Spaghetti plots of core isertels from SH summer months with maximum positive (red)

579   and negative (blue) SAM indices since 1979. (a) Daily JRA-55 core isertels from June 2009, the

580   June with the most positive SAM in the record. (b) As for Fig. 10a but for June 1992, the June

581   with the most negative SAM in the record. (c) As for Fig. 10a but for July 1998. (d) As for Fig.

582   10b but for July 1995. (e) As for Fig. 10a but for August 1994. (f) As for Fig. 10b but for

583   August 1981. Average ALD for the given months are listed in the bottom left of each panel.

584

585   Fig. 11 500 hPa height differences between the composite waviest and least wavy (a) polar jet

586   and (b) subtropical jet seasons constructed from the JRA-55 reanalysis. See Table 1 for

587   identification of the specific years comprising each composite. Positive (negative) height

588   differences are in solid red (blue) lines labeled in m and contoured every 10 m (-10 m) beginning

589   at 10 m (-10 m).

590

591   Fig. 12 250 hPa height differences between the composite waviest and least wavy (a) polar jet

592   and (b) subtropical jet seasons constructed from the JRA-55 reanalysis. See Table 1 for

593   identification of the specific years comprising each composite. Positive (negative) height

594   differences are in solid red (blue) lines labeled in m and contoured every 10 m (-10 m) beginning

595   at 10 m (-10 m).

596

597   Fig. 13 50 hPa height differences between the composite waviest and least wavy (a) polar jet

598   and (b) subtropical jet seasons constructed from the JRA-55 reanalysis. See Table 1 for

599   identification of the specific years comprising each composite. Positive (negative) height

600   differences are in solid red (blue) lines labeled in m and contoured every 10 m (-10 m) beginning

601   at 10 m (-10 m).

602

603
604
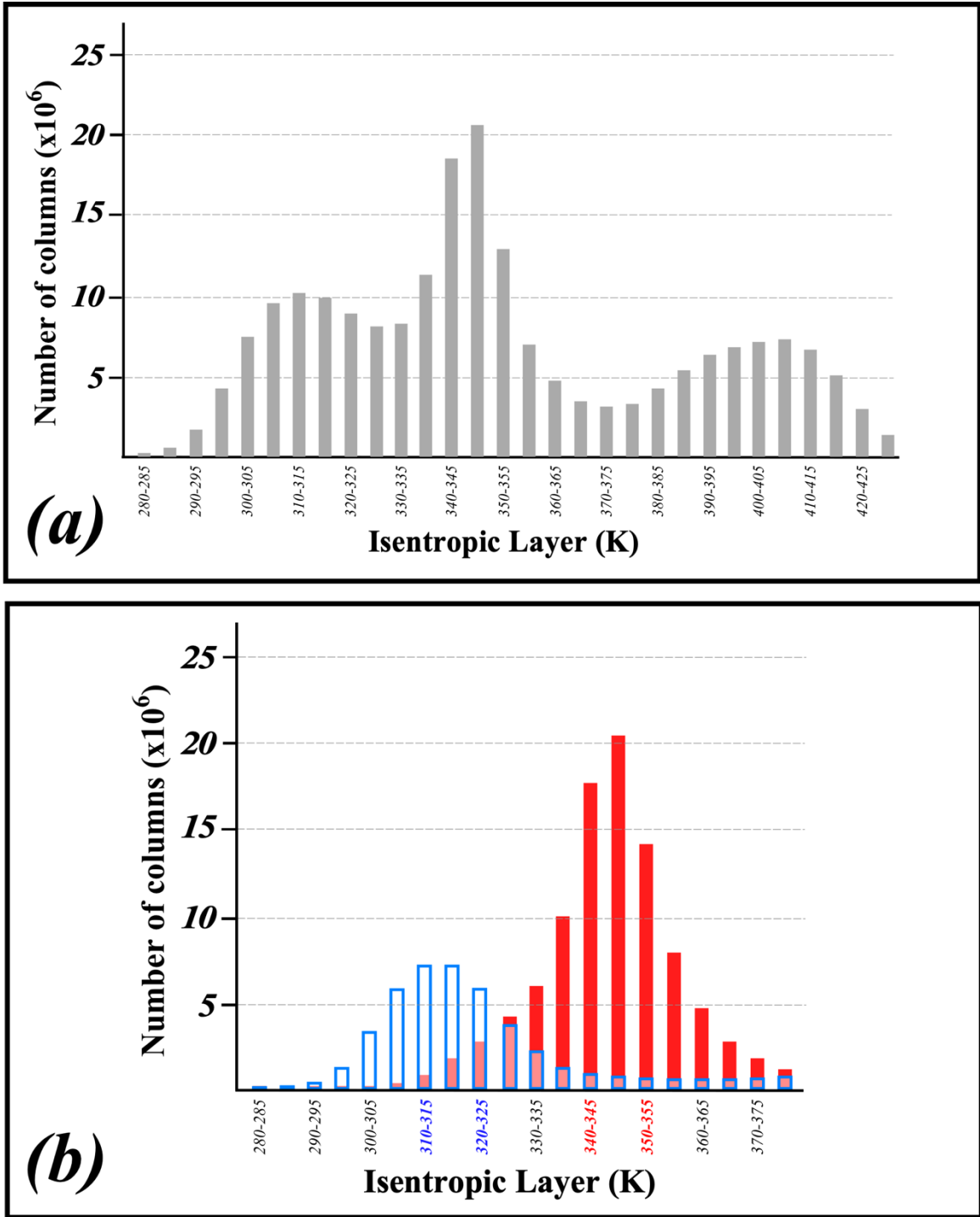
Fig. 1 (a) Distribution of grid-column maximum wind speeds found in 5K isentropic layers from 10 - 80°S for every 6h analysis time in JJA from 1958-2019 from the JRA-55 reanalysis. (b) As for Fig. 1a except limited to (i) grid-columns in which the integral average wind speed from 400 to 100 hPa exceeded 30 m s⁻¹ and (ii) to latitudes 0 - 40°S for the STJ and (iii) latitudes 40 to 65°S for the POLJ.
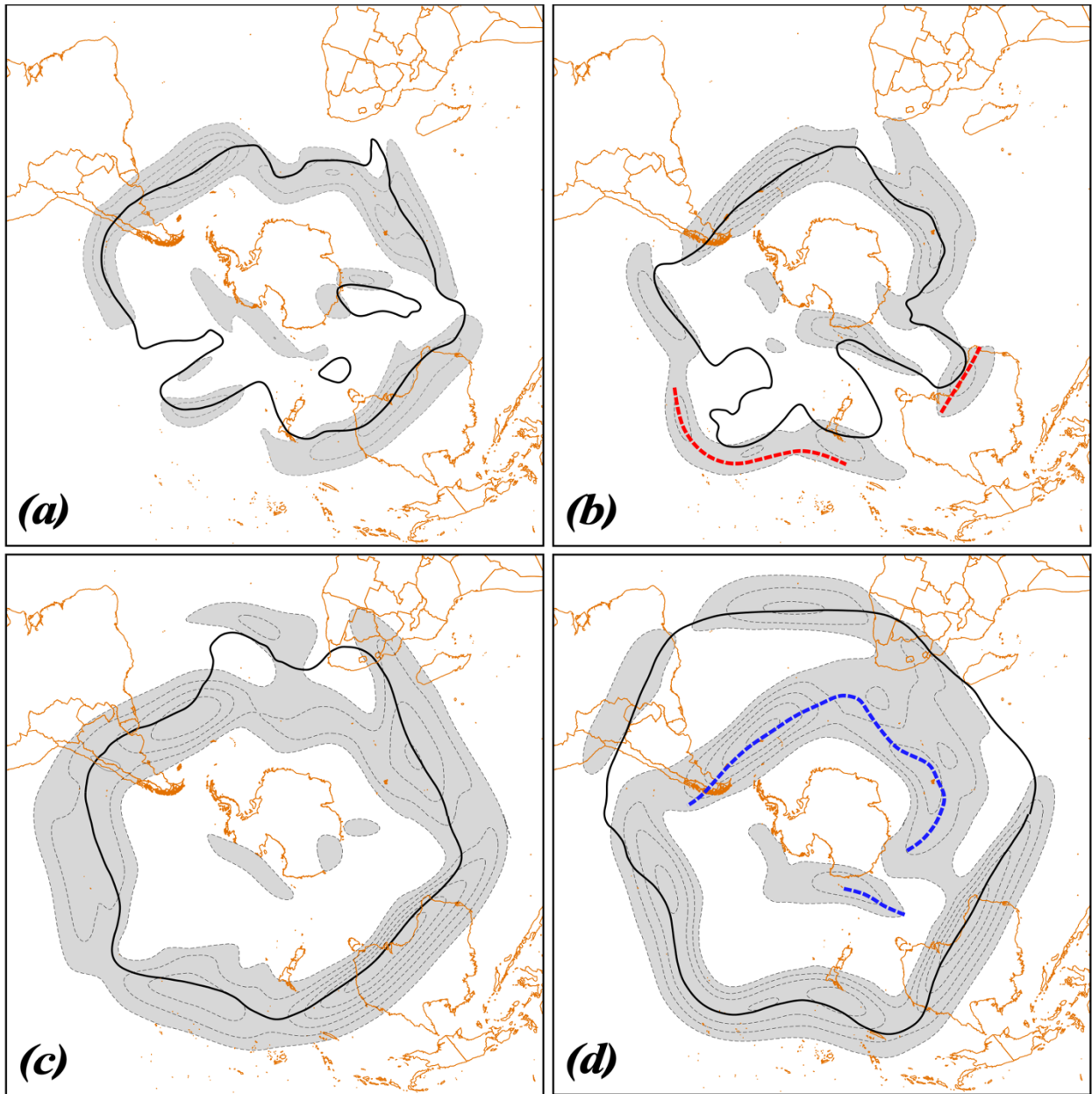
Fig. 2 (a) Isotachs of the daily averaged wind speed (contoured every 10 ma-1 and shaded above 30 m s-1) and the core isertel (bold black line) in the 310:325K isentropic layer on 13 July 1995 from the JRA-55 reanalysis data. The core isertel value is -1.3 PVU. (b) As in (a) but for 24 August 2001. Core isertel value is -2.0 PVU. Dashed red line indicates portion of the core isertel from the overlying STJ layer (depicted in Fig. 2d). (c) As in (a) but for wind speeds and core isertel in the 340:355K isentropic layer on 13 July 1995. Core isertel value is -3.6 PVU. (d) As in (c) but for 24 August 2001. Core isertel value is -1.4 PVU. Dashed blue line indicates a portion of the core isertel from the underlying POLJ layer (depicted in Fig. 2b). See text for further explanation.

606

607

608

609
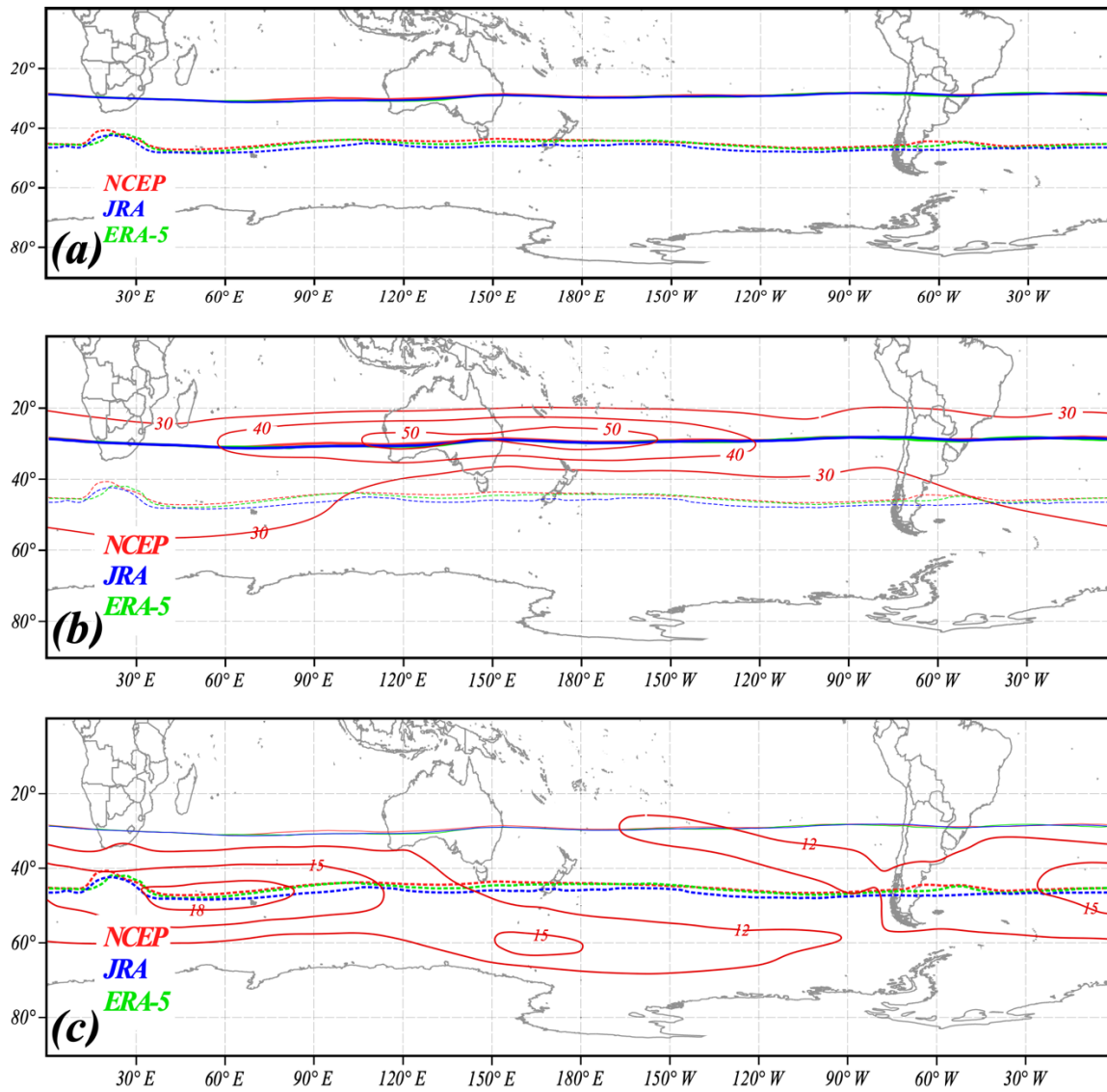
Fig. 3 (a) Solid (dashed) lines are the positions of the average core isertels of the STJ (POLJ) from each of the three reanalyses employed in this study. The different reanalyses are color coded. (b) Thick solid lines are the positions of the average core isertels for the STJ from each of the reanalyses superimposed with JJA average 200 hPa isotachs from the NCEP-NCAR reanalysis. (c) Thick dashed llines are the positions of the average core isertels for the POLJ superimposed with JJA average 700 hPa isotachs from the NCEP-NCAR reanalysis.
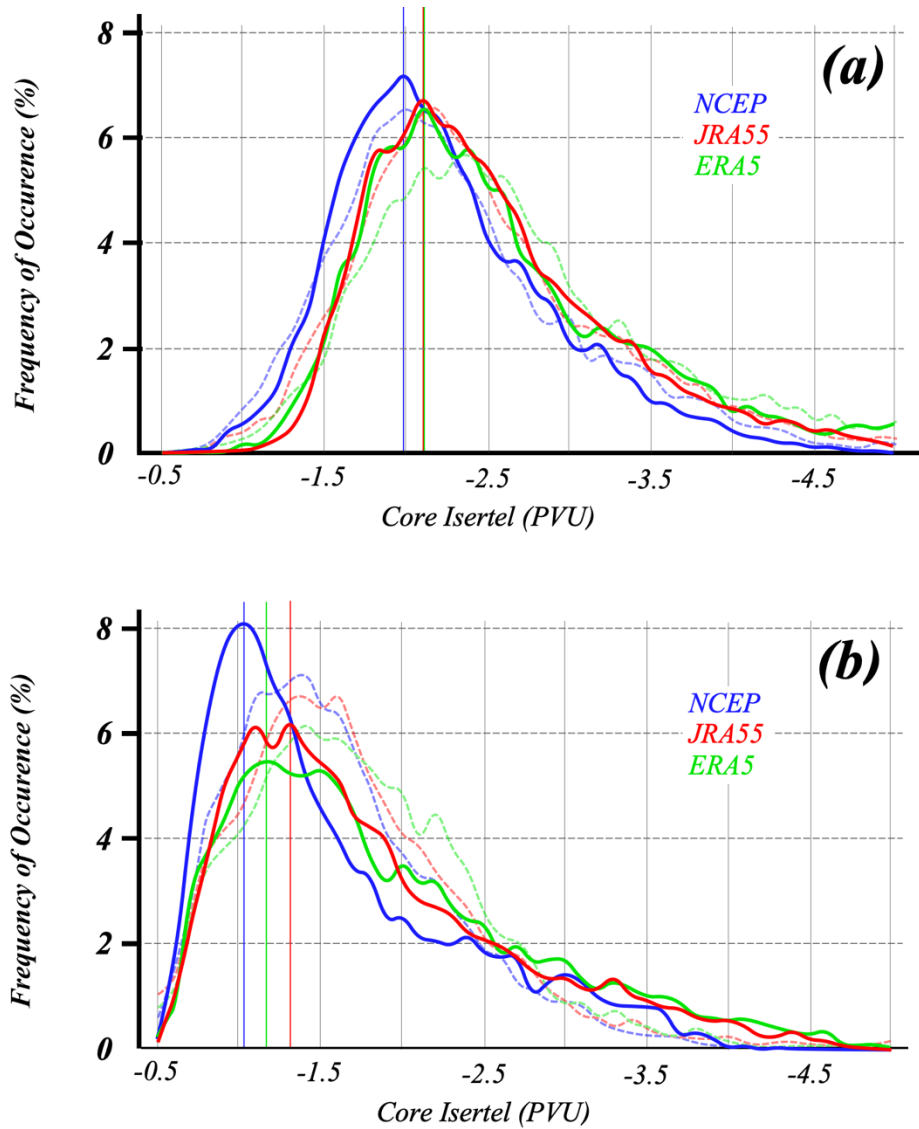
Fig. 4 Frequency of occurrence of the core isertel value for each reanalysis time series in (a) the STJ layer and (b) the POLJ layer. Solid blue, red and green lines in (a) and (b) are the SH distributions from the NCEP, JRA55 and ERA5, respectively. The dashed blue, red and green lines are the NH distributions from the NCEP, JRA55 and ERA5 reanalyses, respectively. In (b), the NH distributions are from the 315:330K layer which houses the POLJ in the boreal winter. Thin blue, red and green lines in (a) and (b) indicate the peak values of the core isertel in each layer from each data set. Isertel values are given in potential vorticity units (PVU, 1 PVU = 10^6 K m^2 kg^{-1} s^{-1}) and are multplied by -1 for the NH values.

610

611
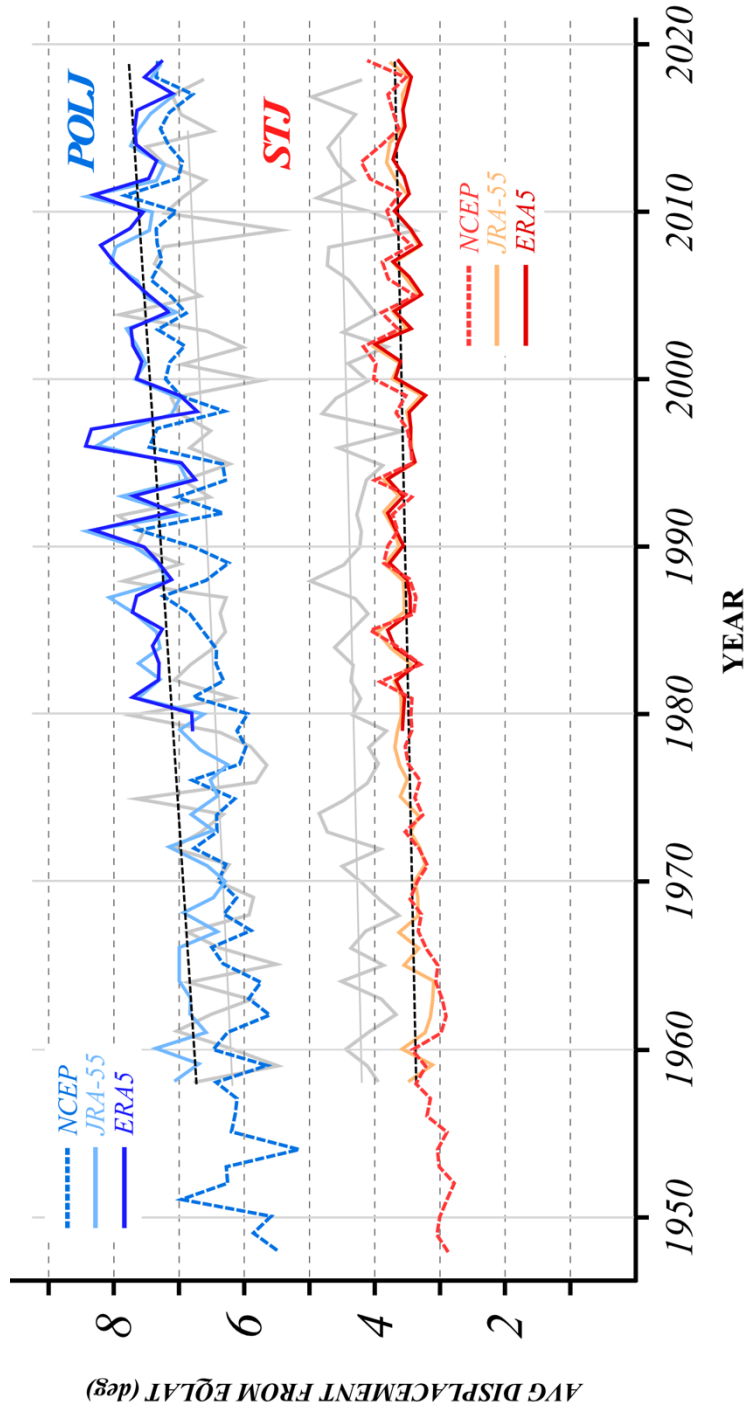
Fig. 5 Seasonal average ALD (in degrees) of the SH wintertime subtropical and polar jets for each cold season in the three reanalysis time series. The polar jet values are in the three shades of blue while the subtropical jet values are in the three shades of red. The dashed black line through each time series represents the trend line for each (derived from the JRA-55 time series) and is significant at the 96% level. Gray line is the boreal winter average ALD from 1958 onward portrayed in Fig. 6 of Martin (2021).The "YEAR" on the abscissa indicates the year in which December of that cold season occurred.
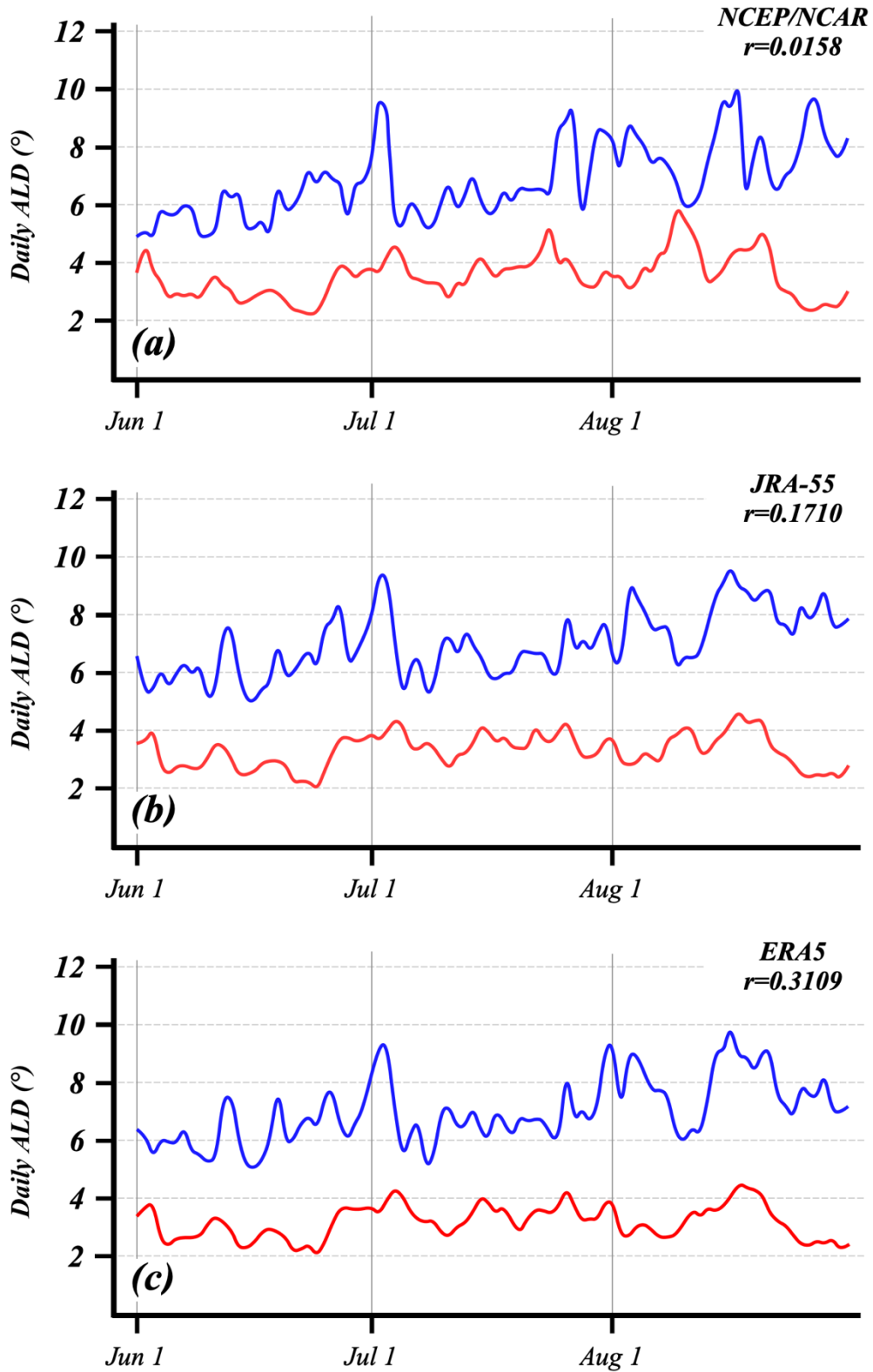
612

Fig. 6 Time series of the daily ALD of the polar (blue lines) and subtropical (red lines) jets from the (a) NCEP-Reanalysis, (b) JRA-55, and (c) ERA5 data sets for austral winter 1999. The correlation between the two times series from each data set is indicated.

613

614

615
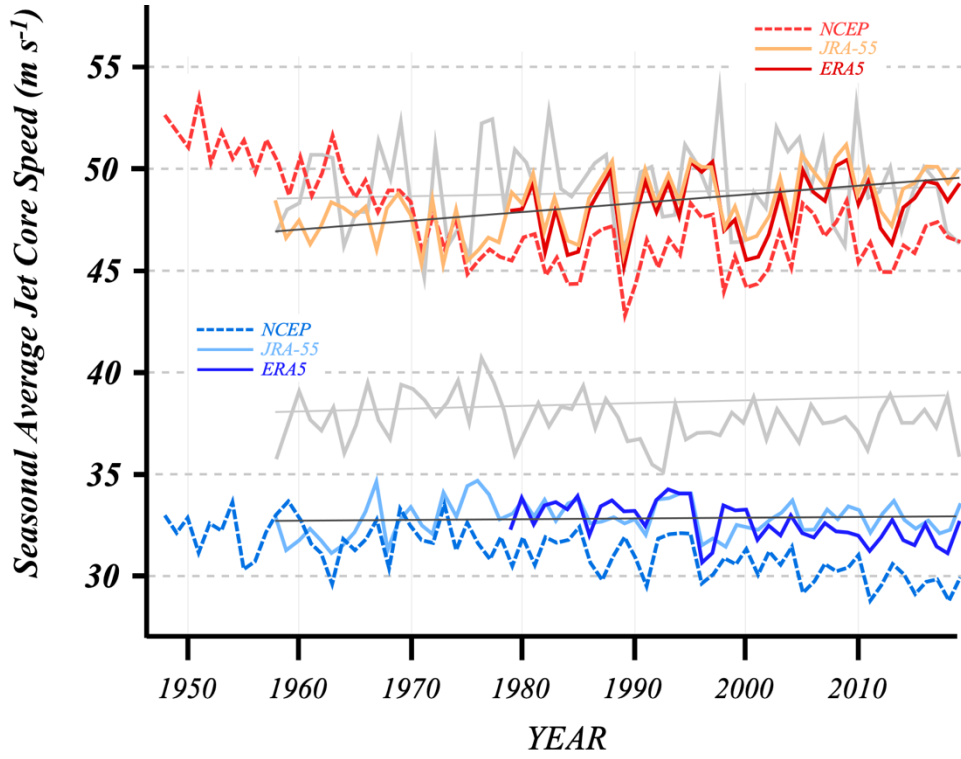
Fig. 7 Seasonal average **U** along the core isertel for the subtropical (red lines) and polar (blue lines) jets from each of the three SH reanalysis data sets. The thin black lines are trend lines for each time series from the JRA-55 data. Gray line is the average (1958-2018) boreal winter **U** analysis for each jet from the three data sets in Fig. 9 of Martin (2021).

616
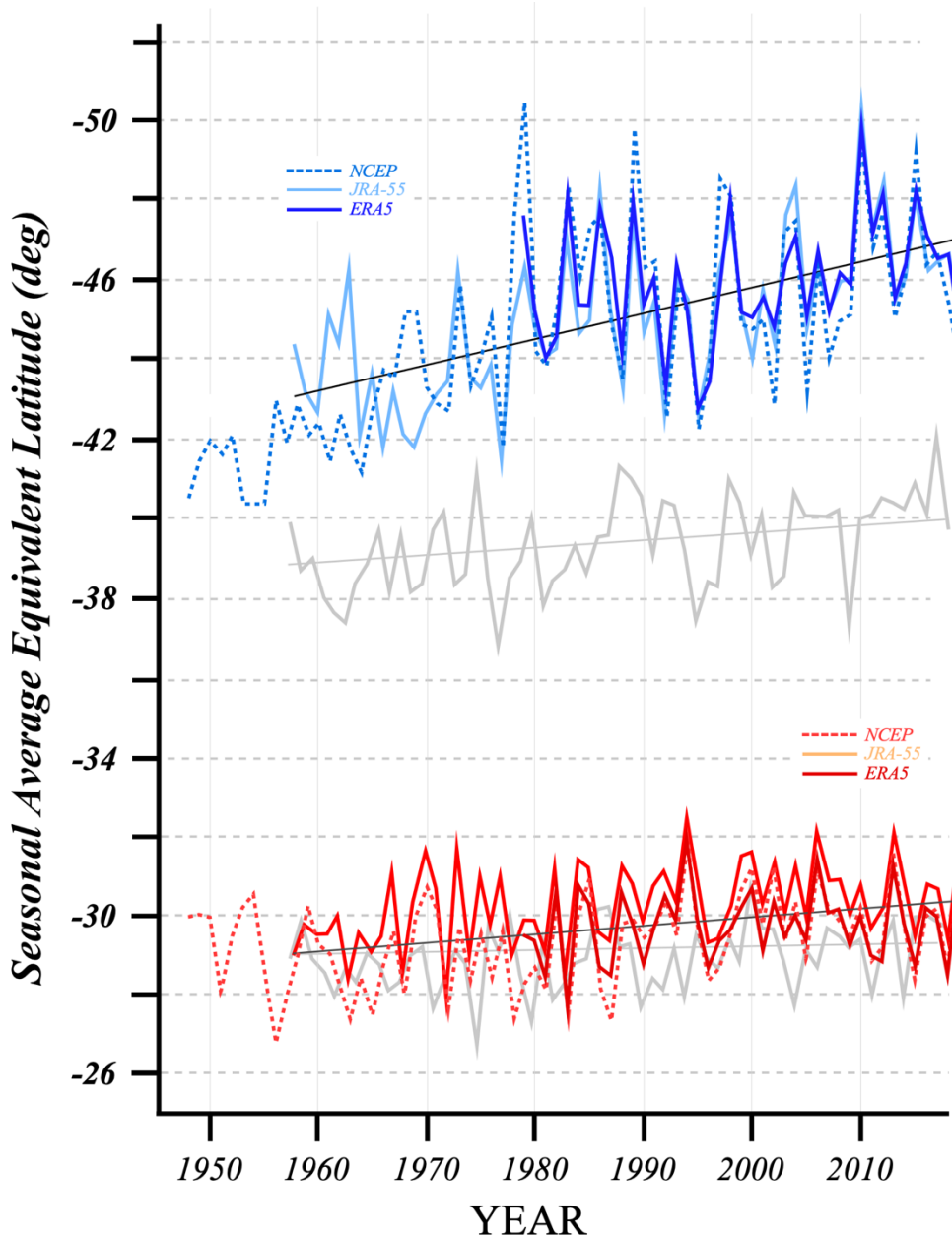
617
618
619
620

Fig. 8 Time series of the seasonal average equivalent latitude of the polar (blue lines) and subtropical (red lines) jets from the three different SH reanalysis data sets. The thin black lines are the trend lines (from the JRA-55 data) and are significant abov e the 99% level for both jet species. Gray line is the boreal winter average (1958-2017) equivalent latitude for each jet from the three reanalysis data sets portrayed in
621 Fig. 10 of Martin (2021).
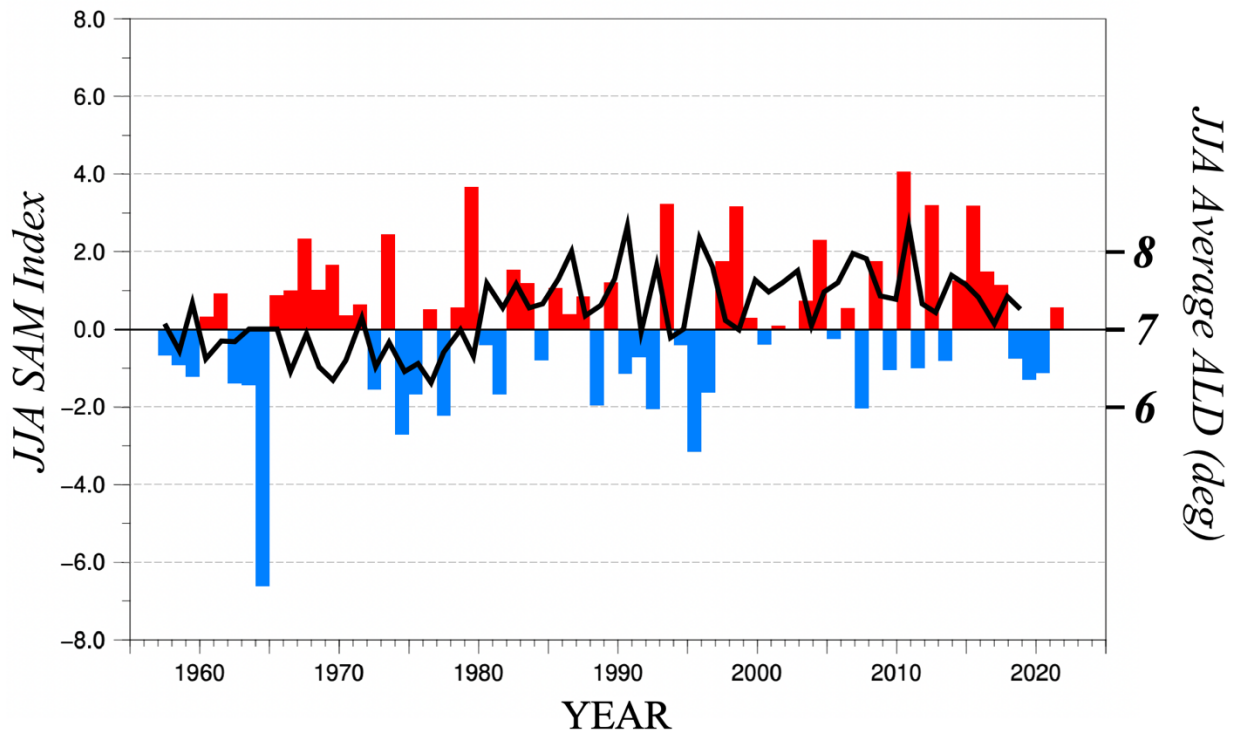
Fig. 9 JJA average SAM index (histogram) from NCEP's Climate Prediction Center. The index is calculated by projecting the daily 700 hPa geopotential height anomalies poleward of 20S onto the leading pattern of the Antarctic Oscillation (AAO) ofGong and Wang (1999). Black solid line is the JJA average ALD of the POLJ from the JRA-55 reanalysis.

622
623
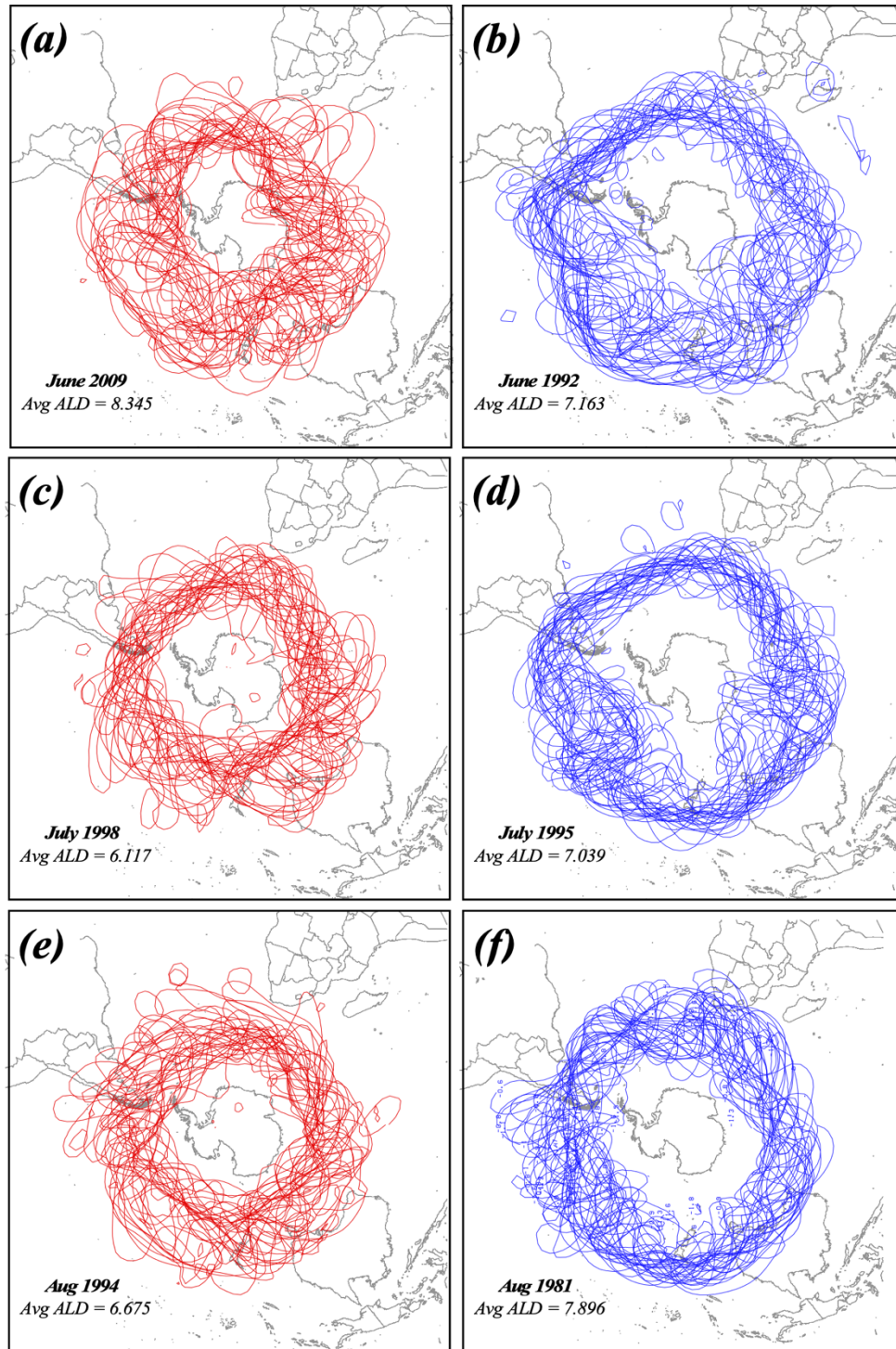
Fig. 10 Spaghetti plots of core isertels from SH summer months with maximum positive (red) and negative (blue) SAM indices since 1979. (a) Daily JRA-55 core isertels from June 2009, the June with the most postive SAM in the record. (b) As for Fig. 10a but for June 1992, the June with themost negative SAM in the record. (c) As for Fig. 10a but for July 1998. (d) As for Fig. 10b but for July 1995. (e) As for Fig. 10a but for August 1994.(f) As for Fig. 10b but for August 1981. Average ALD for the given months are listed in the bottom left of each panel.
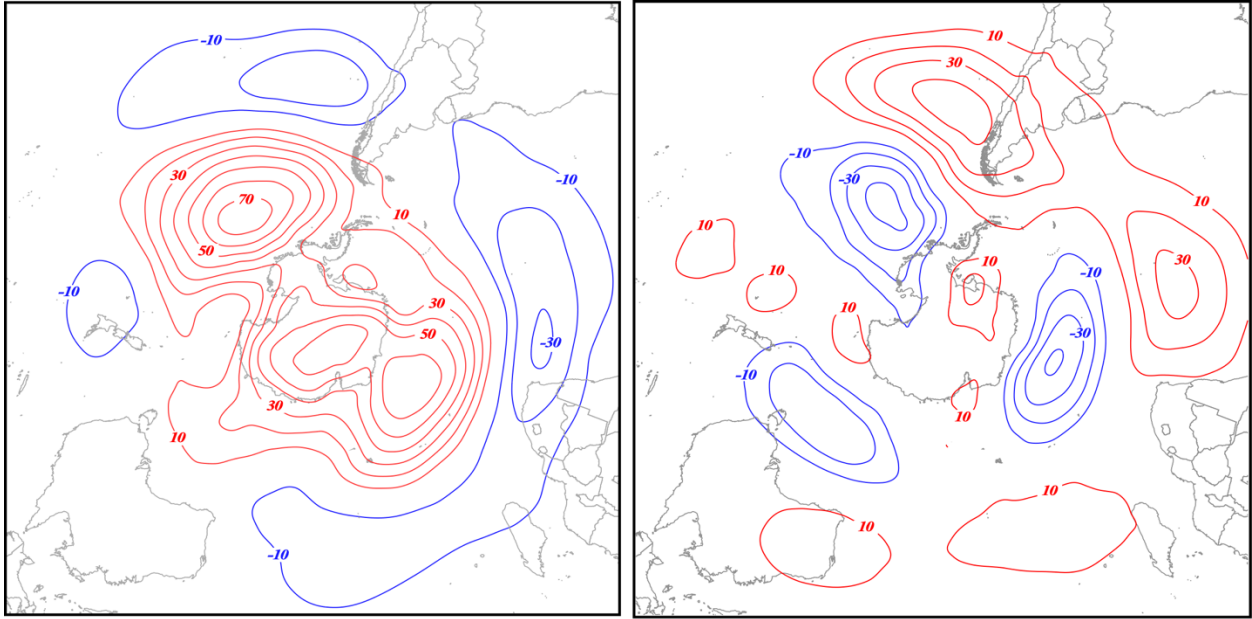
624

Fig. 11 500 hPa height differences between the composite waviest and least wavy (a) polar jet and (b) subtropical jet seasons constructed from the JRA-55 reanalysis. See Table 1 for identification of the specific years comprising each composite. Positive (negative) height differences are in solid red (blue) lines labeled in m and contoured every 10 m (-10 m) beginning at 10 m (-10 m).

625

626

627

628
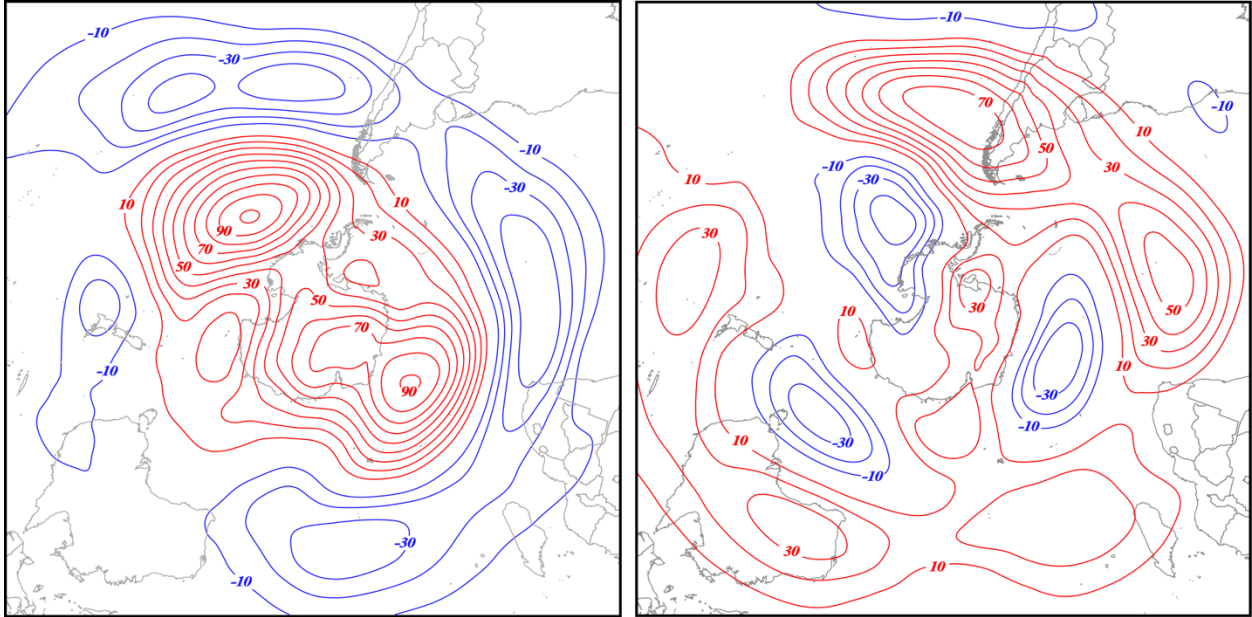
Fig. 12 250 hPa height differences between the composite waviest and least wavy (a) polar jet and (b) subtropical jet seasons constructed from the JRA-55 reanalysis. See Table 1 for identification of the specific years comprising each composite. Positive (negative) height differences are in solid red (blue) lines labeled in m and contoured every 10 m (-10 m) beginning at 10 m (-10 m).

629

630

631

632

Fig. 13 50 hPa height differences between the composite waviest and least wavy (a) polar jet and (b) subtropical jet seasons constructed from the JRA-55 reanalysis. See Table 1 for identification of the specific years comprising each composite. Positive (negative) height differences are in solid red (blue) lines labeled in m and contoured every 10 m (-10 m) beginning at 10 m (-10 m).

633